RSC Advances

PAPER

View Article Online
View Journal | View Issue

Cite this: *RSC Adv.*, 2015, **5**, 908

Ultraviolet photodetector based on heterojunction of n-ZnO microwire/p-GaN film

Meng Ding,[a] Dongxu Zhao,*[b] Bin Yao,[c] Zhipeng Li[d] and Xijin Xu*[a]

Received 25th September 2014
Accepted 26th November 2014

DOI: 10.1039/c4ra11163j

www.rsc.org/advances

High quality ZnO microwires have been fabricated by chemical vapor deposition method. Ultraviolet photodetector based on heterojunction of n-ZnO (individual microwire)/p-GaN film was fabricated. The current–voltage characteristic of the photodetector was investigated, which showed that the heterojunction had rectifying behavior with rectification ratio ($I_{forward}/I_{reverse}$) of about 6.3×10^2 at 4 V. The photoresponse spectrum displayed a sharp cut-off at the wavelength of 380 nm, and the photoresponsivity was as high as 0.45 A W^{-1} at 0 V and 1.3 A W^{-1} at 2.5 V reverse bias. The ultraviolet-visible rejection ratio (R370 nm/R450 nm) is three orders of magnitude under zero bias.

1. Introduction

In recent years, extensive efforts have been made to develop various devices based on semiconductors such as photodetectors, phototransistors, solar cells and others.[1–4] Ultraviolet (UV) photodetectors based on wide band gap semiconductor materials have attracted much attention due to their various applications in commercial and military applications. For example, UV photodetectors can be used in space communications, ozone layer monitoring and flame detection.[5–7] Furthermore, semiconductor UV photodetectors with wide band gap have some advantages, such as the large UV-visible rejection ratio; compared with those with narrow band gap, which exhibit wide photoresponse spectrum covering UV and visible region and low responsivity in the UV region, such as Si ($E_g = 1.12$ eV).

As a wide-band-gap (3.37 eV) multifunctional semiconductor with large exciton binding energy (60 meV), ZnO has triggered much more interest in electronic and optoelectronic applications, such as light-emitting diodes, laser diodes, solar cells, photodetectors and so on.[8–11] Compared with other oxide semiconductors, ZnO-based UV photodetectors can exhibit extremely resistant to high energy proton irradiation and endure harsh radiation for much longer time, so it can be used for space applications. Until now, various architectures of ZnO-based UV photodetectors have been assemblied, such as the p–n junction photodiodes,[11–15] Schottky junction photodiodes,[16–18] photoconductive type.[19,20] Usually, ZnO displays n-type conductivity due to its native defect, such as zinc interstitials and oxygen vacancies. Moreover, it is difficult to obtain reliable and reproducible p-type ZnO due to the low dopant solubility, the deep acceptor level and the "self-compensation" of shallow acceptors resulting from native donor defects. Consequently, different p-type semiconductors, such as Si,[11] NiO,[12] GaN,[13] CuSCN,[14] SiC[15] and so on, have been chosen to fabricate the p–n heterojunction UV photodetectors with ZnO architectures. These photodetectors with p–n junction type have high sensitivity, fast response speed, low dark current and can work without applied bias compared with the photoconductor detectors. Furthermore, these assembly processes of ZnO-based photodetector can avoid complex techniques such as photolithography. Therefore, the p–n heterojunction detector based on ZnO microwire is expected as the most promising candidates for photodetector.

In this paper, the n-ZnO/p-GaN heterojunction photodetector in ultraviolet band was prepared on sapphire substrate, in which the commercial GaN layer grown on sapphire substrate served as the holes injection layer. The *I–V* characteristic of heterojunction photodetector was investigated at room temperature, and the photoresponse properties of individual ZnO microwire based photodetector are discussed in detail.

2. Experiments

ZnO microwires were fabricated by chemical vapor deposition method in a horizontal tube furnace. A mixture of ZnO and graphite powder (1 : 1 in weight) was loaded in alumina boat serving as the source material. The ZnO buffer layer was deposited on the Si substrate by radio frequency magnetron sputtering method at 400 °C. The substrate (ZnO/Si) was laid above the source material with a vertical distance of 4 mm. The whole experiment was in the protection of a constant flow of

[a]*School of Physics and Technology, University of Jinan, 336 Nanxinzhuang west Road, Jinan, 250022, People's Republic of China. E-mail: sps_xuxj@ujn.edu.cn*

[b]*Laboratory of Excited State Processes, Changchun Institute of Optics, Fine Mechanics and Physics, Chinese Academy of Sciences, Changchun 130021, People's Republic of China. E-mail: zhaodx@ciomp.ac.cn*

[c]*Department of Physics, Jilin University, Changchun 130023, People's Republic of China*

[d]*Materials Characterization Group, Western Digital Company, 44100 Osgood Road, California 94539, USA*

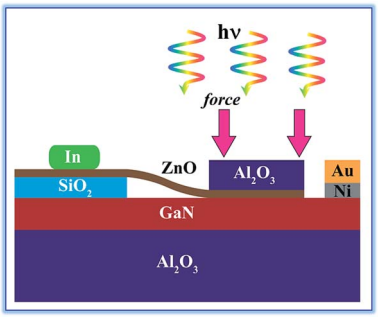

Fig. 1 The schematic illustration of heterojunction photodetector based on individual ZnO microwire/p-GaN film.

Argon (99.99%) with a flow rate of 100 SCCM (SCCM denotes cubic centimeter per minute at standard temperature and pressure). The temperature was heated to 1030 °C at a speed of 20 °C min^{-1}, and kept the temperature for 30 min. Then, the substrate was cooled down to room temperature, the ultralong microwires were found on the substrate and inside the boat.

A schematic diagram of heterojunction photodetector based on individual ZnO microwire/p-GaN film is shown in Fig. 1. Commercial GaN layer grown on sapphire substrate with holes concentration of 1.4×10^{16} cm^{-3} serves as p-type material. The heterojunction photodetector is fabricated as follows: firstly, SiO_2 thin film was deposited on part of GaN film by radio frequency magnetron sputtering for 30 min. Secondly, one end of individual ZnO microwire was fixed on SiO_2 thin film by indium electrode, while the other end of individual ZnO microwire was fixed on the GaN film without SiO_2. The Ni/Au metal layers were deposited on p-GaN layer by vacuum evaporation in order to form ohmic contact, respectively.

The morphology and structure of as-grown ZnO microwires were characterized by the field emission scanning electron microscopy (FESEM) and transmission electron microscopy (TEM). The optical absorption spectra of ZnO microwires and GaN film were recorded using a Shimadzu UV-3101PC spectrophotometer at room temperature. The photoluminescence (PL) spectrum of individual ZnO microwire was measured in a JY-630 micro-Raman spectrometer using He–Cd laser (325 nm) as excitation source. The current *versus* voltage characteristics of the detector was performed using a Hall measurement system (Lake Shore 7707). The photoresponse of the device was detected using a standard lock-in technique (EG&G 124A), monochromator, chopper (EG&G 192), and a 150 W Xe lamp as an excitation light source.

3. Results and discussion

Fig. 2a shows the typical FESEM image of as-grown individual ZnO microwire. The average diameter and length of ZnO microwire is about several microns and 1 cm, respectively. TEM image (Fig. 2b) shows that ZnO microwire has four laterals with tetragonum section. The HRTEM (Fig. 2c) result indicates that the lattice fringe is about 0.26 nm corresponding to the {0002} plane of wurtzite ZnO. The corresponding selected area electron diffraction pattern (Fig. 2d) proves the nanowire to be crystalline. The EDX data (from the red circle of Fig. 2e) shown in Fig. 2f indicates that the sample is composed of O, Zn elements without any impurities. The Cu element comes from the copper grid of measurement.

Fig. 3 shows the absorption spectra of commercial GaN film layer and ZnO microwires at room temperature, respectively. For p-GaN film, a steep absorption edge at 364 nm is observed as shown in Fig. 3a, from which the optical band gap can be deduced to be 3.4 eV. The absorption spectrum of ZnO microwire (Fig. 3b) presents an absorption edge at 381 nm, which is consistent with the band gap of ZnO.

Optical characterization method has advantage for defect characterization of the materials because it does not require physical contact. In particular, the low-temperature PL emission peaks are sensitive for the defect states. The room temperature PL spectra of the ZnO microwire and GaN film are shown in Fig. 4a. A dominant emission peak at 385 nm is observed for individual ZnO microwire, which is corresponding to the near band edge emission of ZnO. In addition, defect emission generally attributed to structural defects, single ionized vacancies, and impurities in visible region is absent,

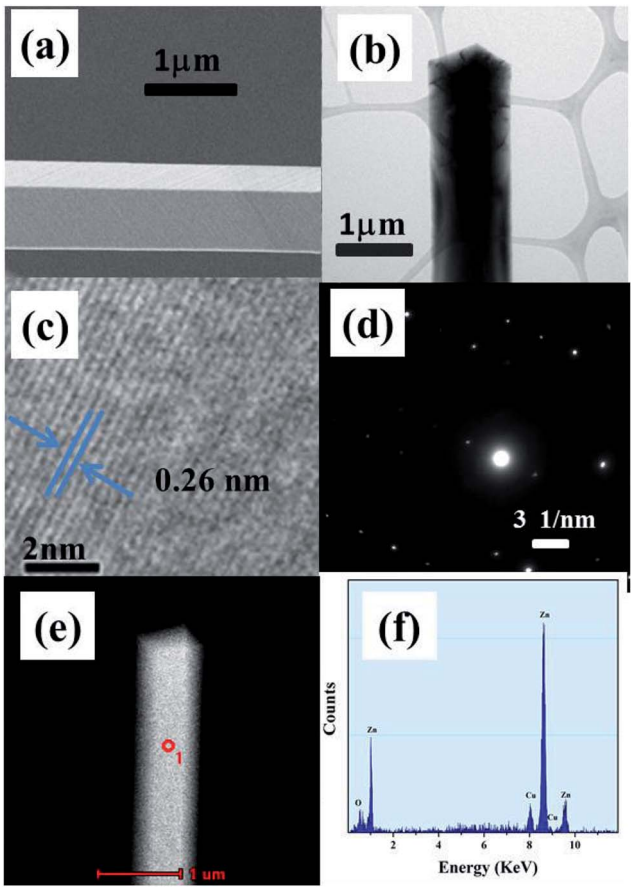

Fig. 2 (a) SEM image of individual ZnO microwire. (b) Low-magnification TEM image of individual ZnO microwire. (c) HRTEM image of ZnO microwire. (d) A SAED pattern taken on this ZnO microwire. ((e) and (f)) EDS spectrum shows the composition of Zn and O element.

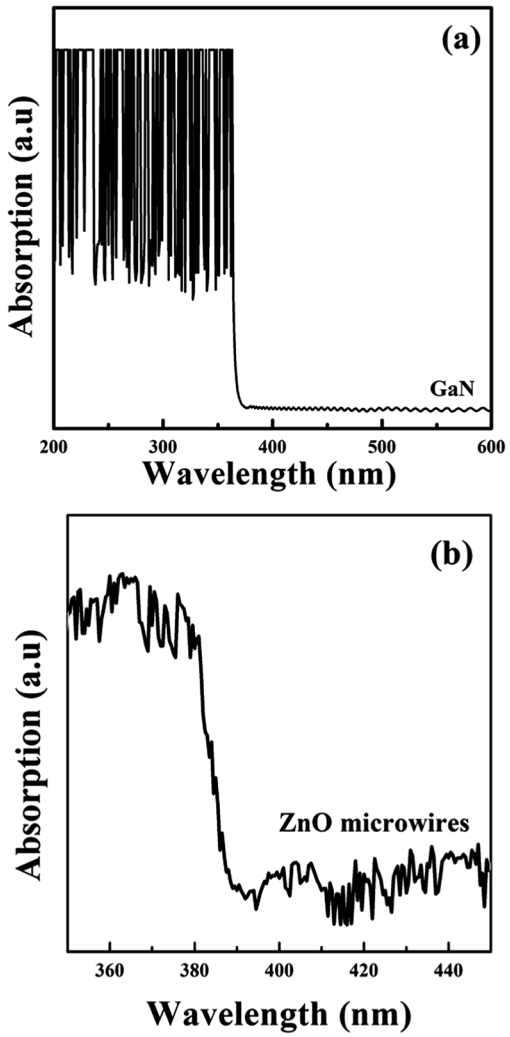

Fig. 3 Absorption spectra obtained at room temperature of GaN film (a) and ZnO microwires (b), respectively.

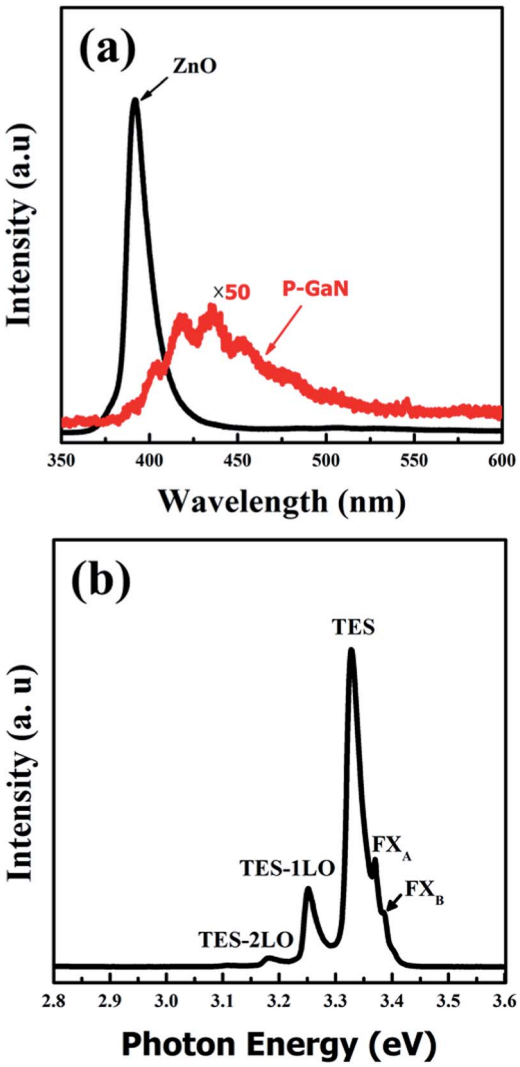

Fig. 4 (a) The photoluminescence spectra of GaN film and individual ZnO microwire at room temperature. (b) Low temperature PL spectra of individual ZnO microwire performed at 83 K.

which suggests the ZnO microwire is of high crystal quality. In order to further certify the high optical quality of microwire, the low temperature PL spectrum (83 K) is performed, as shown in Fig. 4b. The peaks centred at 3.385 eV and 3.370 eV can be ascribed to the type-B exciton (FX_B) and the type-A exciton (FX_A) emissions of ZnO, respectively.[21,22] The peak at 3.327 eV can be attributed to two-electron satellite (TES) transition, which is characteristic of the neutral-donor-bound exciton transition in the spectral region of 3.32–3.34 eV.[23] The two peaks at 3.253 eV and 3.181 eV are assigned to the longitudinal optical (LO) phonon replicas of TES transition, because the energy separation between them is 70 meV consistent with the energy of optical phonon. In the PL spectrum of GaN film, a broad peak at about 440 nm was dominant, which is attributed to the transition from conduction band electrons or shallow donors to Mg acceptors. Moreover, the fringes observed in the spectrum are due to the thin film interference of the emitted light reflected by GaN/air and the sapphire/GaN interfaces.[24,25]

Fig. 5 shows the current–voltage (I–V) characteristic of the n-ZnO/p-GaN heterojunction photodetector. The measurement was performed in the bias voltage range of −13 to 10 V. In term of the I–V curve, the heterojunction shows obvious rectifying behavior with rectification ratio ($I_{forward}/I_{reverse}$) of about 6.3 × 10^2 at 4 V, indicating the formation of a diode. The threshold voltage and the reverse leakage current is about 3 V and 2.07 × 10^{-7} A (under 4 V reverse bias), respectively. The ideality of the diode can be determined from the diode equation,[26]

$$I = I_s\left[\exp\left(\frac{eV}{nkT}\right) - 1\right] \quad (1)$$

where I_s is the reverse saturation current, k is the Boltzmann constant, T is the absolute temperature, e is the elementary electric charge, V is the applied voltage, and n is the ideality factor. The ideality factor obtained is larger than 2, also the deviation from the ideal value is probably attributed to high contact resistance between GaN and ZnO caused by the physical contact.

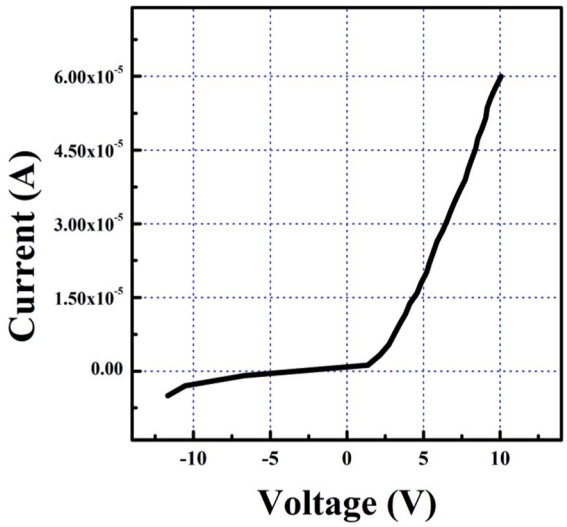

Fig. 5 The current–voltage curve of n-ZnO microwire/p-GaN heterojunction.

To investigate the UV-sensing properties of n-ZnO microwire/p-GaN heterojunction, photoresponse property under reverse bias (−2.5 V) and without bias were also measured at room temperature. The typical response curves of the heterojunction photodetector are shown in Fig. 6, which display high photoresponsivity to UV radiation. The detector responsivity $R(\lambda)$is calculated by the formula:

$$R(\lambda) = I(\lambda)/P(\lambda) \quad (2)$$

where $P(\lambda)$ is the power of incident light, which changes with wavelength. When the applied bias is zero, the peak responsivity of the photodetector is about 0.45 A W^{-1}, also the UV-visible rejection ratio (R370 nm/R450 nm) of the photodetector is about three orders of magnitude, as shown in the response spectra, which indicates that the photodetector exhibits relatively high signal-to-noise ratio. When the reverse bias increases to 2.5 V, the peak responsivity of the photodetector is about 1.3 A W^{-1} at 370 nm, and the cut-off wavelength is located at 380 nm, which corresponds to the band gap of ZnO consistent with the result of PL measurement at room temperature. In addition, the UV-visible rejection ratio (R370 nm/R450 nm) of the photodetector is about two orders of magnitude. The dark current is little at zero voltage, it will increase with applied reverse bias, so the R370 nm/R450 nm under 0 V is higher than that at −2.5 V. When the wavelength of incident light decreases, that is to say that the photon energy increases, then the absorption coefficient increases, so the penetration depth of light becomes shallower. The shorter penetration depth of light in the wavelength region will induce the decrease of responsivity from 380 nm to 300 nm results as discussed in previous reports.[27,28]

The photoresponse mechanism of this heterojunction detector can be explained using the energy band diagram according to Anderson's model and the carrier diffusion process,[29] as shown in Fig. 7. The band gap value of ZnO and GaN are 3.37 eV and 3.39 eV at room temperature, respectively, and the electron affinity of the two semiconductors are 4.35 eV (ZnO), 4.20 eV (GaN).[30,31] When the ZnO and p-GaN are contacted, a small conduction band offset and valence band offset are observed. The conduction band offset ΔE_c can be figured out as: $\Delta E_c = \chi(\mathrm{ZnO}) - \chi(\mathrm{GaN}) = 0.15$ eV, and the valence band offset ΔE_v is obtained by $\Delta E_v = E_g(\mathrm{ZnO}) - E_g(\mathrm{GaN}) + \Delta E_c = 0.13$

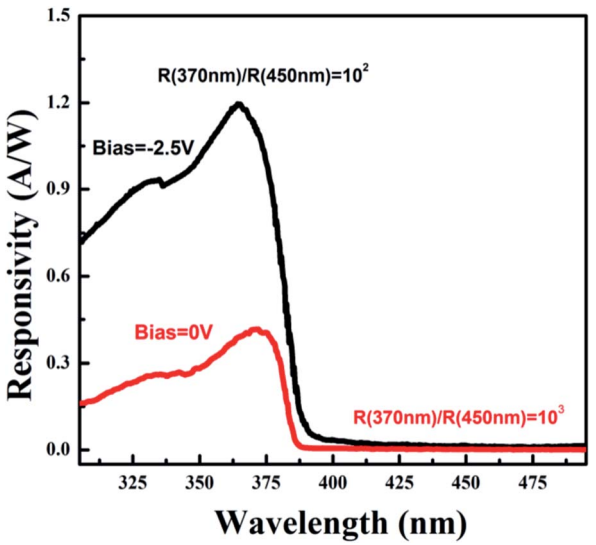

Fig. 6 Room-temperature response of the n-ZnO microwire/p-GaN photodetector at 0 and −2.5 V.

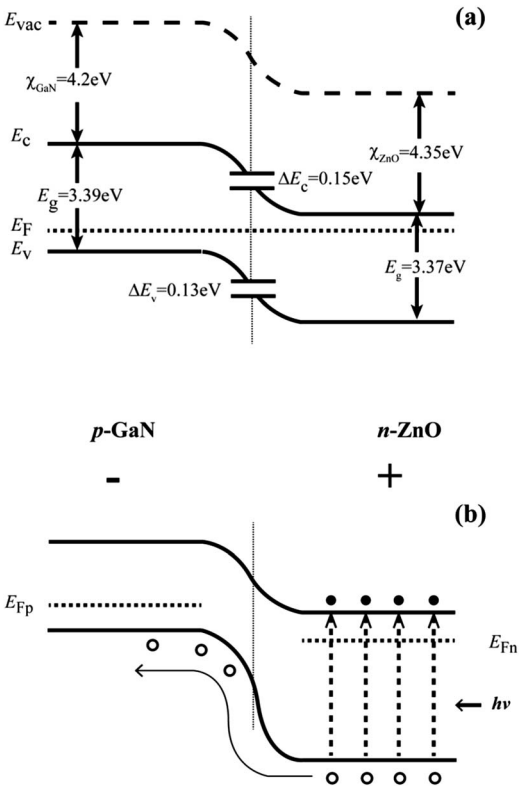

Fig. 7 The energy band diagram of the n-ZnO/p-GaN heterojunction without applied bias (a), and reverse bias (b), respectively.

eV. To express the spectral responses bias at zero voltage, the energy band diagrams of the heterojunction is shown in Fig. 6b. When the heterojunction is irradiated by the ultraviolet light, the photon with energy larger than bandgap will be absorbed. Then electrons–hole pairs are photoinduced and greatly increase the concentration of minority carriers. The build-in electric field drives the photogenerated electrons near or in the junction region toward ZnO side, while photogenerated holes shift to the opposite direction. Eventually, photocurrent signal can be obtained. When the heterojunction is applied with reverse bias (a positive bias is applied on the ZnO microwire), the energy diagram is displayed in Fig. 6b. The electric field caused by reverse bias in depletion region is consistent with the build-in electric field, so the barrier height is enhanced. The photogenerated electrons are confined in the ZnO side by the strong electric field. Meanwhile, the photogenerated holes drift easier toward GaN compared with that without bias, so it's more advantageous to seperate photogenerated hole and electrons. Therefore, photocurrent signals will be enhanced in this case, giving good photoresponse signal in the UV band.

4. Conclusion

In summary, individual n-ZnO microwire/p-GaN heterojuction photodetector has been fabricated. The UV photoresponse result shows that the device has a good UV response sensitivity. Under illumination conditions, the photodiode displays a high UV responsivity of 0.45 A W^{-1} at zero bias. When the reverse bias increases to 2.5 V, the responsivity peak of the photodetector is about 1.3 A W^{-1} at 370 nm. The photoresponse spectrum indicates a visible blind UV detectivity with sharp cut-off of responsivity at the wavelength of 380 nm, which corresponds to the near band edge absorption of ZnO. An UV-visible rejection ratio (R370 nm/R450 nm) of three orders of magnitude was obtained at reverse bias of zero V. These results display that the photodetector exhibits relatively high signal-to-noise ratio.

Acknowledgements

This work is supported by National Basic Research Program of China (973 Program) under Grant no 2011CB302004, the National Natural Science Foundation of China (Grant no. 11304120, 11304121), the Encouragement Foundation for Excellent Middle-aged and Young Scientist of Shandong Province (Grant no. BS2012CL005, BS2013CL020), Doctoral foundation of University of Jinan (UJN) (Grant no. XBS1326). Thanks University of Jinan (UJN) for the support on new staff, and the project supported by the Taishan Scholar (no. TSHW20120210).

References

1 X. S. Fang, L. F. Hu, K. F. Huo, B. Gao, L. J. Zhao, M. Y. Liao, P. K. Chu, Y. Bando and D. Golberg, *Adv. Funct. Mater.*, 2011, **21**, 3907.
2 J. P. Lu, H. W. Liu, S. Z. Deng, M. R. Zheng, Y. H. Wang, J. A. V. Kan, S. H. Tang, X. H. Zhang, C. H. Sow and S. G. Mhaisalkar, *Nanoscale*, 2014, **6**, 7619.
3 J. F. Wang, M. S. Gudiksen, X. F. Duan, Y. Cui and C. M. Lieber, *Science*, 2001, **293**, 1455.
4 J. P. Lu, J. H. Lu, H. W. Liu, B. Liu, K. X. H. Chan, J. D. Lin, W. Chen, K. P. Loh and C. H. Sow, *ACS Nano*, 2014, **8**, 6334.
5 M. Razeghi and A. Rogalski, *J. Appl. Phys.*, 1996, **79**, 7433.
6 Y. A. Goldberg, *Semicond. Sci. Technol.*, 1999, **14**, 41.
7 H. Ohta and H. Hosono, *Mater. Today*, 2004, **7**, 42.
8 O. Lupan, T. Pauporté and B. Viana, *Adv. Mater.*, 2010, **22**, 3298.
9 Y. P. Li, X. Y. Ma, L. Jin and D. R. Yang, *J. Mater. Chem.*, 2012, **22**, 16738.
10 L. Etgar, J. S. Bendall, V. Laporte, M. E. Welland and M. Graetzel, *J. Mater. Chem.*, 2012, **22**, 24463.
11 A. Baltakesmez, S. Tekmen, P. Köç, S. Tüzemen, K. Meral and Y. Onganer, *AIP Adv.*, 2013, **3**, 032125.
12 P. N. Ni, C. X. Shan, S. P. Wang, X. Y. Liu and D. Z. Shen, *J. Mater. Chem. C*, 2013, **1**, 4445.
13 H. Zhu, C. X. Shan, B. Yao, B. H. Li, J. Y. Zhang, D. X. Zhao, D. Z. Shen and X. W. Fan, *J. Phys. Chem. C*, 2008, **112**, 20546.
14 S. M. Hatch, J. Briscoe and S. Dunn, *Adv. Mater.*, 2012, **25**, 867.
15 Y. I. Alivov, Ü. Özgür, S. Dogan, D. Johnstone, V. Avrutin, N. Onojima, C. Liu, J. Xie, Q. Fan and H. Morkoç, *Appl. Phys. Lett.*, 2005, **86**, 241108.
16 G. Cheng, X. H. Wu, B. Liu, B. Li, X. T. Zhang and Z. L. Du, *Appl. Phys. Lett.*, 2011, **99**, 203105.
17 J. Dai, C. X. Xu, X. Y. Xu, J. Y. Guo, J. T. Li, G. Y. Zhu and Y. Lin, *ACS Appl. Mater. Interfaces*, 2013, **5**, 9344.
18 X. W. Fu, Z. M. Liao, Y. B. Zhou, H. C. Wu, Y. Q. Bie, J. Xu and D. P. Yu, *Appl. Phys. Lett.*, 2012, **100**, 223114.
19 D. Park and K. Yong, *J. Vac. Sci. Technol., B: Microelectron. Nanometer Struct.–Process., Meas., Phenom.*, 2008, **26**, 1933.
20 K. W. Liu, J. G. Ma, J. Y. Zhang, Y. M. Lu, D. Y. Jiang, B. H. Li, D. X. Zhao, Z. Z. Zhang, B. Yao and D. Z. Shen, *Solid-State Electron.*, 2007, **51**, 757.
21 J. N. Dai, H. C. Liu, W. Q. Fang, L. Wang, Y. Pu, Y. F. Chen and F. Y. Jiang, *J. Cryst. Growth*, 2005, **283**, 93.
22 F. Y. Jiang, J. N. Dai, L. Wang, W. Q. Fang, Y. Pu, Q. M. Wang and Z. K. Tang, *J. Lumin.*, 2007, **122**, 162.
23 Ü. Özgür, Y. I. Alivov, C. Liu, A. Teke, M. A. Reshchikov, S. Doğan, V. Avrutin, S. J. Cho and H. Morkoç, *J. Appl. Phys.*, 2005, **98**, 041301.
24 H. Zhu, C. X. Shan, B. Yao, B. H. Li, J. Y. Zhang, Z. Z. Zhang, D. X. Zhao, D. Z. Shen, X. W. Fan, Y. M. Lu and Z. K. Tang, *Adv. Mater.*, 2009, **21**, 1613.
25 J. Dai, C. X. Xu and X. W. Sun, *Adv. Mater.*, 2011, **23**, 4115.
26 S. Mridha and D. Basak, *J. Appl. Phys.*, 2007, **101**, 083102.
27 D. G. Zhao, D. S. Jiang, J. J. Zhu, Z. S. Liu, S. M. Zhang, J. W. Liang, H. Yang, X. Li, X. Y. Li and H. M. Gong, *Appl. Phys. Lett.*, 2007, **90**, 062106.
28 S. M. Sze, *Physics of Semiconductor Devices*, Wiley, New York, 2nd edn, 1981, ch. 13, p. 750.
29 S. M. Sze, *Physics of Semiconductor Devices*, Wiley, New York, 2nd edn, 1981.
30 J. A. Aranovich, D. G. Golmayo, A. L. Fahrenbruch and R. H. Bube, *J. Appl. Phys.*, 1980, **51**, 4260.
31 M. C. Jeong, B. Y. Oh, M. H. Ham and F. Myoung, *Appl. Phys. Lett.*, 2006, **88**, 202105.

